Advances in Geo-Energy Research

Vol. 20, No. 2, p. 129-144, 2026

Original article

Dynamic optimization control of injection-production parameters for autothermic pyrolysis *in-situ* conversion process of oil shale

Chaofan Zhu[1], Cheng He[1], Jiyue Wu[2], Wei Guo[1]*

[1]*State Key Laboratory of Deep Earth Exploration and Imaging, College of Construction Engineering, Jilin University, Changchun 130026, P. R. China*

[2]*Petroleum Recovery Research Center (PRRC), New Mexico Institute of Mining and Technology, Socorro 87801, United States*

Keywords:
Oil shale
autothermic pyrolysis
injection-production parameters
numerical simulation
dynamic regulation

Cited as:
Zhu, C., He, C., Wu, J., Guo, W. Dynamic optimization control of injection-production parameters for autothermic pyrolysis *in-situ* conversion process of oil shale. Advances in Geo-Energy Research, 2026, 20(2): 129-144.
https://doi.org/10.46690/ager.2026.05.03

Abstract:
The autothermic pyrolysis *in-situ* conversion process of oil shale has emerged as a vital development direction due to its advantages of environmental friendliness and low cost. However, previous studies predominantly employed constant injection and production parameters, which often result in inefficient compression energy injection and formation oxidation losses, thereby limiting further improvements in energy efficiency and oil production. To address these issues, this study establishes a dynamic optimization model for injection-production parameters in the autothermic pyrolysis *in-situ* conversion process of oil shale, developing a dynamic control methodology for gas injection rate and oxygen content to enhance the economic viability and feasibility of the process. The results indicate that under the optimal combination of gas injection – adjustment time, decay rate, and terminal flow rate – the steady-state phase during late production can significantly reduce input compression energy and inhibit hydrocarbon oxidation losses, ultimately leading to a substantial increase in the peak energy efficiency and cumulative oil production. Furthermore, by synergistically regulating oxygen content and injection rate during the early production stage, the compression energy can be further reduced, ultimately elevating the energy efficiency to approximately fourteen, demonstrating the technical feasibility for industrial-scale production. These findings and the identified key parameters provide crucial theoretical and technical support for the large-scale application of the autothermic pyrolysis *in-situ* conversion technology for oil shale.

1. Introduction

Oil shale as a sedimentary rock that is rich in kerogen releases substantial recoverable hydrocarbons through pyrolytic retorting, making it a significant unconventional hydrocarbon resource (Xie et al., 2020; Wang et al., 2024a, 2024b). Globally, oil shale reserves are abundant, with the estimated recoverable shale oil resources far exceeding those of conventional petroleum and other unconventional hydrocarbons, potentially meeting global energy demands for decades (Xie et al., 2020; Wang et al., 2024a). Many countries with rich oil shale resources but limited conventional oil and gas reserves regard its efficient development as strategically critical for alleviating energy supply pressures and enhancing energy security (Li et al., 2025a, 2025b). Contemporary oil shale exploitation is predominantly categorized into two principal technical methodologies: surface retorting and *in-situ* conversion (Jin et al., 2025; Wang et al., 2025). Conventional surface retorting processes are characterized by significant

Yandy Scientific Press

*Corresponding author.
E-mail address: chaofan_zhu@jlu.edu.cn (C. Zhu); hecheng24@mails.jlu.edu.cn (C. He); jiyue.wu@nmt.edu (J. Wu); guowei6981@jlu.edu.cn (W. Guo).

Received March 3, 2026; revised March 29, 2026; accepted April 15, 2026; available online April 17, 2026.

environmental challenges and are predominantly constrained to shallow geological formations. In contrast, *in-situ* conversion technology demonstrates enhanced environmental compatibility, reduced surface land occupancy, improved economic viability, and suitability for medium to deep reservoir development, establishing it as a critical developmental pathway for industrial-scale implementation in this sector (Wu et al., 2024).

Globally, over ten distinct technological approaches for the *in-situ* conversion of oil shale have been established, with representative methods including Shell's In-Situ Conversion Process (Brandt, 2008; Pei et al., 2018), Chevron's CRUSH technology (Liu et al., 2022), ExxonMobil's Electrofrac technology (Jia and Huang, 2024), Jilin University's autothermic pyrolysis *in-situ* conversion process (Guo et al., 2024), and Taiyuan University of Technology's steam-assisted *in-situ* conversion technology (Lu et al., 2022). Among them, the autothermic pyrolysis *in-situ* conversion process involves locally preheating the target oil shale formation, followed by injecting oxygen-containing gases to initiate oxidation reactions with residual kerogen pyrolysis products, thereby generating sustained heat for formation heating. Guo et al. (2023a) analyzed the heating mechanism and reaction zone characteristics of this technology, demonstrating its superior energy efficiency compared to conventional electrical heating methods and dividing the reaction process into five distinct zones. Yang et al. (2023b) experimentally investigated the effects of oxygen concentration and gas flow rate on an autothermal retorting system, identifying an optimal parameter set of 16% oxygen content and 5 L/min flow rate, which achieved an oil yield of 67.1% and an energy efficiency of 3.46. Xu et al. (2023) optimized the autothermic pyrolysis *in-situ* conversion process (ATS) through temperature control, revealing that oil shale pyrolysis at 300-450 °C produces bitumen and volatile oils, with semicoke calorific value peaking at 330 °C. They recommended a preheating temperature range of 350-370 °C and a pyrolysis temperature of 422-492 °C. Furthermore, Gao et al. (2022) demonstrated that optimizing air injection rate, oxygen concentration, and fracture spacing can significantly enhance shale oil recovery.

The ATS significantly reduces external energy input, demonstrating clear advantages in cost control (Wang et al., 2025). However, the current laboratory experiments and numerical simulations of this process predominantly employ fixed operational parameters (e.g., gas flow rate, oxygen concentration, pressure), with lab-scale studies achieving an energy efficiency of merely 3.46, insufficient for large-scale commercialization. Thus, the primary challenges can be summarized as follows: (1) While complex fracture networks created by hydraulic fracturing enhance reservoir permeability, injected gases often fail to fully participate in pyrolysis reactions due to gas channeling (He et al., 2024) and heterogeneous fracture connectivity (Ma et al., 2023), leading to additional compression energy losses, which are particularly evident during the early and late production stages; (2) During air injection, pyrolyzed (especially light) hydrocarbons are prone to oxidation reactions with oxygen (Du et al., 2023), reducing the final oil production. These issues highlight the potential for improvement in both energy efficiency and oil production for autothermic pyrolysis technology. Future optimization should focus on the dynamic regulation of injection-production parameters to mitigate gas channeling losses, suppress hydrocarbon oxidation, and shorten preheating duration, thereby advancing the commercial viability of this process.

To address the limitations of conventional constant-rate or single-parameter control modes that result in suboptimal energy efficiency and oil productions, this study aims to enhance the economic viability and technical feasibility of the autothermic pyrolysis *in-situ* conversion process of oil shale by constructing a dynamic optimization model for injection-production parameters. Firstly, an optimal constant-flow-rate parameter is determined through parametric optimization, which serves as the baseline for dynamic regulation. Subsequently, numerical simulations are performed to analyze the impact of different gas injection flow rate variation patterns (including adjustment time, decay rate, and terminal flow rate) on the extraction process. By integrating energy efficiency and hydrocarbon production outcomes, the optimal gas injection parameter combination is identified. Furthermore, to improve reaction initiation efficiency and enhance effective hydrocarbon displacement, a synergistic adjustment of oxygen content and injection rate during the pyrolysis initiation phase is implemented based on the optimized flow rate regulation. Finally, a phased, multi-parameter optimization approach is established to develop a dynamic regulation methodology for injection-production parameters, which simultaneously elevates energy efficiency and hydrocarbon production, providing a theoretical and technical foundation for the large-scale application of this technology.

2. Mathematical model formulation

2.1 Mathematical model and grid discretization

This study employs the CMG STARS^{TM} module to conduct numerical simulations of the autothermic pyrolysis *in-situ* conversion process in oil shale. As illustrated in Fig. 1, an inverted seven-spot well pattern consisting of seven vertical wells is designed. To reduce computational complexity while maintaining model accuracy and experimental reliability, a $1/6$ symmetrical sector of the well pattern – one containing one injection well and two production wells – is modeled. The simulated formation thickness is 0.1 m, with a well spacing of 50 m and a drainage area of 1,083 m^2. Given the tight nature of oil shale formations, autothermic pyrolysis development requires integration with hydraulic fracturing. The simulation assumes a dual-porosity dual-permeability system post-stimulation, with a matrix permeability of 0.01 md and fracture permeability of 100 md (Dong et al., 2018; Wang et al., 2020). A three-dimensional geological model is established through finite difference discretization within a conventional Cartesian coordinate grid system, with grid dimensions of 0.5 m $\times$ 0.866 m $\times$ 0.1 m (Fig. 1). To mitigate the impact of low absolute hydrocarbon production values resulting from the minimal formation thickness (0.1 m) on development evaluation, hydrocarbon production per unit formation thickness (unit: m^3/m) is adopted as a normalized indicator to more effectively reflect production efficiency under varying condi-

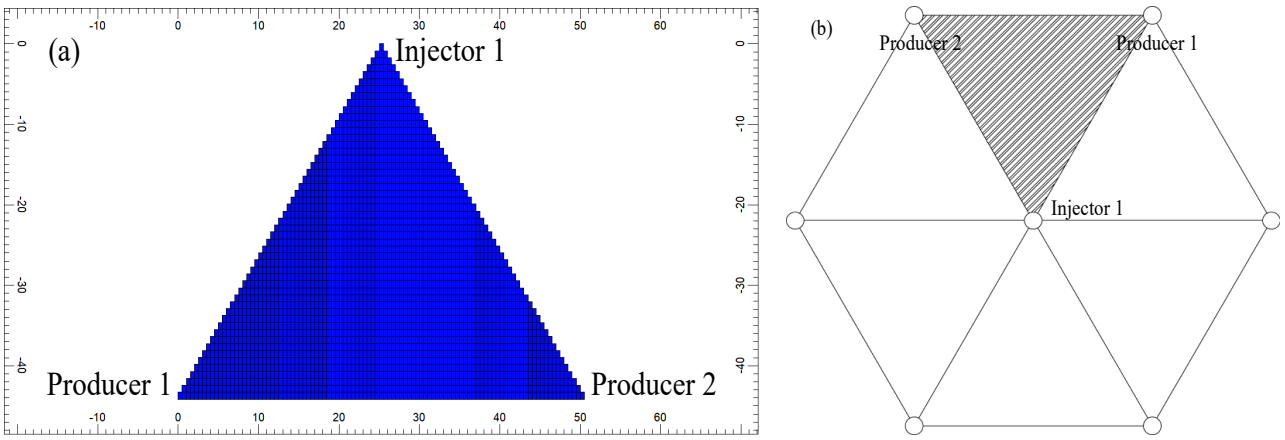

Fig. 1. Geological model: (a) Grid division and (b) well deployment method.

Table 1. Physical characterization parameters of oil shales (Tong et al., 2011; Wang et al., 2019; He et al., 2021; Zhu et al., 2022).

Parameter	Value
Initial formation pressure (kPa)	6,500
Initial formation temperature (°C)	35
Initial formation permeability (md)	0.01
Fracture permeability (md)	100
Original porosity for matrix (%)	6.40
Total porosity (%)	28.65
Matrix specific heat capacity (J/m^3·°C)	1.5×10^6
Matrix thermal conductivity (J/m·day·°C)	1.21×10^5
Rock thermal expansion coefficient (°C^{-1})	3.09×10^{-6}
Density of rock matrix (kg·m^{-3})	2,400
Initial water saturation in the matrix (%)	100
Formation matrix density (kg/m^3)	2,019.84
Kerogen density in the pores (mol/m^3)	6.336×10^4

tions. The injection well operates under constant-pressure mode at 20 MPa, while production wells maintain a bottom-hole pressure of 200 kPa. The gas injection process comprises two stages: (1) A preheating phase injecting 500 °C nitrogen for 7 days to ensure that formation temperature near the injection well exceeds the autothermic pyrolysis reaction threshold; (2) An autothermic pyrolysis reaction phase switching to 25 °C air, with the injection rates and oxygen content dynamically adjusted according to the reaction progress.

The research object of this study is high-quality oil shale from the Songliao Basin in China, which is recognized as one of the world's largest Cretaceous lacustrine basins (Wang, 2013; Yan et al., 2023). The target reservoir interval, identified as the First Member of the Nenjiang Formation, is primarily composed of grayish-black shale and oil shale, which were deposited in deep and semi-deep lacustrine depositional settings. The upper part of this member is covered by gray mudstone of the Second Member of the Nenjiang Formation, while its lower part is composed of green shale and siltstone. The kerogen is predominantly type I–II$_1$, indicating excellent source rock quality. Vitrinite reflectance measurements indicate that the shale is in a low-maturity stage (Fan, 2022; Sun et al., 2022). The initial water saturation in the matrix pores is assumed to be 100%, with a matrix porosity of 6.40% (Shakib et al., 2015; Zhang et al., 2022). The matrix rock is assumed to have a thermal conductivity of 1.21×10^5 J/(m·day·°C) and a heat capacity of 1.50×10^6 J/(m^3·°C) (Guo et al., 2023b), while the kerogen contains a carbon mass fraction of 0.71 and has a molecular weight of 14.7 g/mol. The kerogen porosity in the shale is 22.2%, with a kerogen concentration of 6.336×10^4 mol/m^3 in the pores. The organic matter exhibits low thermal maturity, evidenced by a mean random vitrinite reflectance (R_0) value of 0.5%, which is conducive to light hydrocarbon generation. Quantitative mineralogical analysis indicated that quartz constitutes the predominant phase (54%), followed by illite (20%) and calcite (6%) as subordinate components (Zhu et al., 2022). The analyzed oil shale sample displays a free hydrocarbon (S1) content of 1.21 mg/g, classifying it as a low-maturity source rock. In contrast, the pyrolyzable hydrocarbon (S2) content is significantly higher at 110.06 mg/g, denoting an exceptional hydrocarbon-generating capacity. Furthermore, the residual carbon (S4) content of 108.35 mg/g reveals that substantial residual pyrolysis potential remains after primary hydrocarbon generation and expulsion (Guo et al., 2022). The physical characteristics of the analyzed oil shale are summarized in Tables 1-3.

2.2 Reaction model

Reaction models and kinetic parameters are fundamental prerequisites for numerical simulations, since they characterize the chemical reactions and corresponding rates of organic matter during the heating process (Yang et al., 2023a). During the autothermic pyrolysis of oil shale, kerogen undergoes pyrolysis to yield heavy oil (HO), light oil (LO), hydro-

Table 2. Characterization of organic elemental and mineralogical composition of shale (Zhu et al., 2022).

Organic elemental analysis (%)					Mineral composition (%)							
C	H	O	N	S	Quartz	Alkali feldspar	Plagioclase	Calcite	Pyrite	Pyrite	Kaolinite	Chlorite
72.38	9.72	10.92	4.07	3.91	54	4	7	6	3	20	2	4

Table 3. Oil content analysis and rock-evaluation of shale (Guo et al., 2022).

Oil content analysis (wt%)				Rock evaluation			
Shale oil	Gas	Water	Residue	S1 (mg/g)	S2 (mg/g)	S4 (mg/g)	TOC (%)
14.52	6.98	5.76	72.74	1.21	110.06	108.35	16.9

carbon gas (HC), and prechar, whose subsequent pyrolysis yields additional hydrocarbon gas and residual carbon (Tian et al., 2025; Zhao et al., 2025; Jin et al., 2026). Furthermore, all organic components can undergo oxidation reactions with oxygen (Zhao et al., 2023). At temperatures below 350 °C, low-temperature oxidation (LTO) occurs, involving oxidative addition reactions of kerogen and bond scission reactions in light oil (LO) and hydrocarbon gas (HC). High-temperature oxidation (HTO) involves bond cleavage reactions of HO, LO, HC, and prechar (Alshareef et al., 2011). The chemical reaction models for all organic species are summarized in Table 4. Due to the significant similarities in kerogen type and depositional environment between the Songliao Basin and the Green River oil shale in Colorado, the kinetic parameters (including frequency factor, activation energy and reaction enthalpy) for the primary and secondary cracking reactions, as proposed by the Braun and Burnham model and originally validated in field tests of Green River oil shale, have been applied to the analysis of oil shale from the Songliao Basin (Pei et al., 2018; He et al., 2019; Khakimova et al., 2019). The modified model has been revised to be applicable to the oil shale deposits within the Songliao Basin (Zhu et al., 2022), as shown in Table 4. For oil shale strata exhibiting diverse oil saturations within the Songliao Basin, the reaction kinetics framework, including the governing equations and activation energy parameters, is kept constant. The variability in observed reactivity is attributed exclusively to differences in the initial kerogen concentration. Consequently, the reaction equations detailed in the accompanying table retain their validity and exhibit strong applicability across the varying oil saturation conditions encountered in the basin. These kinetic parameters collectively serve to characterize the rate of the cracking reactions and the associated thermal effects as a function of temperature.

2.3 Energy efficiency

Energy efficiency serves as a primary comprehensive indicator, defined as the ratio of total energy output to energy input throughout the ATS process. The energy conversion within the ATS system is categorized into three distinct parts: (1) Cumulative compression energy of gas injection; (2) cumulative injected thermal energy; and (3) total heating value of the produced fluids.

The specific formula for energy efficiency is:

$$f_t = \frac{N_h^{out} + N_{og}}{N_h^{in} + N_c} \tag{1}$$

where f_t denotes the total energy efficiency; N_c denotes the compression energy of gas injection; N_h^{out} denotes the thermal energy of the gas injected during the preheating stage, kJ; N_{og} denotes the calorific value of the produced hydrocarbons (oil and natural gas), kJ; and N_h^{in} denotes the thermal energy carried by the gas, kJ. Based on previous research (Wang et al., 2018), the heating values for the produced oil and natural gas during the ATS process are conventionally taken as 40.0×10^6 and 35.6×10^3 J/m^3. Consequently, the temporal evolution of energy efficiency throughout the ATS operation is quantified by Eq. (1), with the optimal process termination point defined by the maximum value on the energy efficiency.

2.4 Dynamic regulation methodology

2.4.1 Dynamic gas injection rate

Conventional injection-production processes typically employ a constant-flow-rate injection principle (Yang et al., 2023b). To establish a baseline for subsequent dynamic regulation of gas injection rates, this study first identifies an optimal constant flow rate that yields the highest production efficiency as the control, which all simulation results of dynamic regulation strategies will be compared against. Based on the optimal constant flow rate, numerical simulation and parameter optimization reveal that dynamic gas injection parameters, including adjustment time, decay rate and terminal flow rate, significantly influence the energy efficiency and hydrocarbon production during the autothermic pyrolysis *in-situ* conversion of oil shale. This study employs a phased nested optimization strategy to determine the optimal combination of key parameters. First, the adjustment time (the point at which the gas injection rate declines to the final flow rate) is optimized, followed by the decay rate (the rate at which the gas injection rate decreases) based on the previously determined timing. Finally, the terminal flow rate (the gas injection rate value at the end of the production period) is optimized based on the

Table 4. Kerogen pyrolysis chemical reaction model in oil shale (He et al., 2019; Khakimova et al., 2019; Guo et al., 2023a).

Description	Reaction	Frequency factor (1/s)	Activation energy (kJ/mol)	Reaction enthalpy (kJ/mol)
Kerogen pyrolysis	$CH_{1.45}O_{0.04}N_{0.02}S_{0.01} = 0.0071C_{3.16}H_{8.33} + 0.0097C_{15.26}H_{32.52} + 0.0108C_{27.17}H_{56.34} + 0.6411\text{Prechar}$	3.0×10^{13}	213.50	-4.20
Prechar pyrolysis	$\text{Prechar} = 0.01718C_{3.16}H_{8.33} + 0.9902C$	1.0×10^{13}	226.09	-46.50
Kerogen oxidation	$CH_{1.45}O_{0.04}N_{0.02}S_{0.01} + 0.1052O_2 = 1.4225\text{Prechar}$	6.47×10^{4}	64.32	27.89
Light oil oxidation	$C_{15.26}H_{32.52} + 21.864O_2 = 16.26H_2O + 12.208CO_2 + 3.052CO$	2.61×10^{5}	72.68	7,794.69
Natural gas oxidation	$C_{3.16}H_{8.33} + 4.9296O_2 = 4.164H_2O + 2.5312CO_2 + 0.6328CO$	2.61×10^{5}	72.68	1,758.46
Heavy oil oxidation	$C_{27.17}H_{56.34} + 38.5359O_2 = 28.164H_2O + 21.7368CO_2 + 5.4342CO$	2.57×10^{7}	118.44	13,735.40
Prechar oxidation	$\text{Prechar} + 1.1723O_2 = 0.5750H_2O + 0.78152CO_2 + 0.19538CO$	6.02×10^{8}	133.91	454.84
Residual carbon oxidation	$C + 0.9O_2 = 0.8CO_2 + 0.2CO$	6.02×10^{8}	133.91	315.80

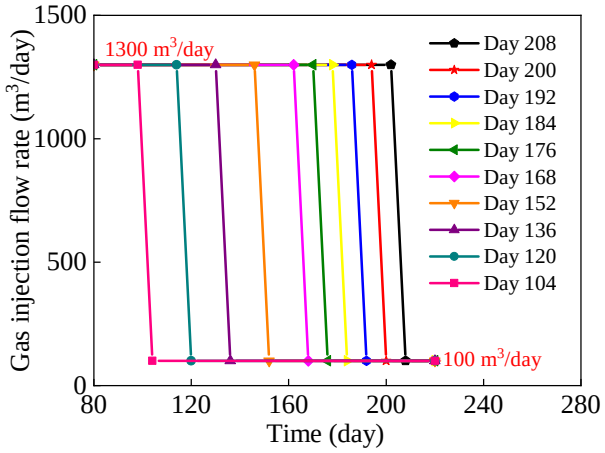

Fig. 2. Flow rate function under different adjustment times.

results of the first two steps, thereby ultimately forming an optimal three-parameter control combination of adjustment time, decay rate and terminal flow rate through progressive optimization. This combination is designed to maintain high energy efficiency, achieved by substantially reducing the gas injection rate during the peak production period of oil and gas. This lowers the cumulative compression energy injected and minimizes the oxidative loss of oil and gas products, thereby significantly improving the energy efficiency.

The optimization of adjustment time window involves identifying the period of peak hydrocarbon generation as well as strategically reducing the gas injection rate within this interval to minimize energy consumption. Fig. 2 illustrates the variation in gas injection rate over time under different adjustment times. The initial injection rate is set to the optimal constant value. After the adjustment time, the flow rate decreases at a preset decay rate of 200 m^3/d^2, reaching a terminal flow rate of 100 m^3/day after 6 days. Each curve represents a distinct adjustment time (i.e., the time point at which flow rate reduction initiates). Premature flow rate reduction may lead to insufficient formation heating, hindering pyrolysis zone expansion. Conversely, delayed adjustment implies continued high-rate gas injection when hydrocarbon production stabilizes and autothermic pyrolysis effects adequately sustain reactions, resulting in unnecessary energy input and the excessive combustion of hydrocarbons. Both scenarios ultimately reduce energy efficiency and hydrocarbon production.

Based on the previously determined optimal adjustment time for gas injection rate, this study further optimizes the key regulation parameter of decay rate. As shown in Fig. 3, the initial and terminal gas injection rates remain unchanged, while the decay rate, which is represented by the absolute value of the slope (k) in the flow rate function, varies within the range of 12.5 to 1,200 m^3/d^2 to achieve different decay speeds. The distinct curves in Fig. 3 correspond to different decay rate settings: A larger absolute slope value indicates a faster flow rate decline, reflecting variations in the intensity and temporal distribution of energy input reduction during regulation. Excessive decay rates may lead to abrupt reservoir pressure drops, impairing fluid displacement efficiency and potentially cooling the reaction zone. Conversely, insufficiently slow decay rates could result in prolonged unnecessary energy input during the decay phase.

Building upon the previously optimized adjustment time and decay rate of gas injection rates, this study further focuses on the third critical parameter – the terminal flow rate. As illustrated in Fig. 4, the initial gas injection rate remains set at the optimal constant value, while the adjustment time and

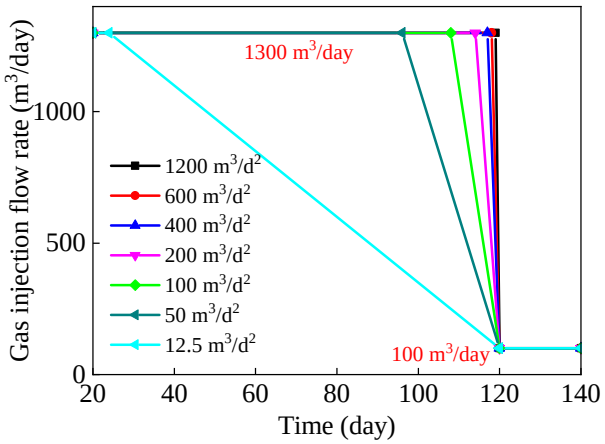

Fig. 3. Flow rate function under different decay rates.

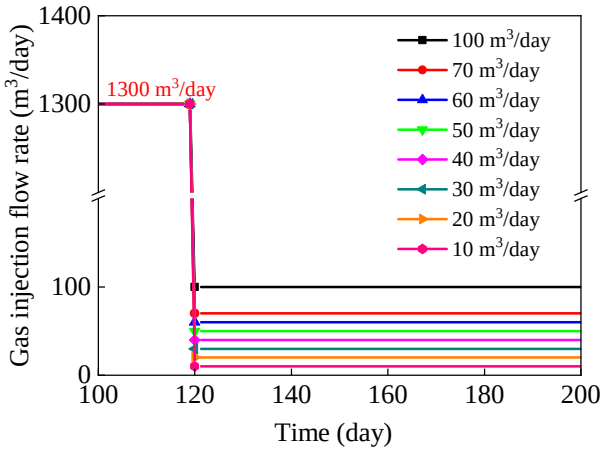

Fig. 4. Flow rate function under different terminal flow rates.

decay rate parameters are fixed at the results from prior optimization. The terminal flow rate (adjusted within 10-100 m^3/day) is systematically investigated to analyze its impact on development performance. During the late-stage autothermic pyrolysis reaction, the kerogen pyrolysis rate slows and its remaining concentration decreases, maintaining an appropriate terminal flow rate that serves dual roles: first, it facilitates the displacement of un-migrated hydrocarbons through sustained gas injection to improve oil recovery; second, it supplies limited oxygen for the oxidation of residual carbon, sustaining minimal autothermic pyrolysis reactions to prolong the production capacity release period. However, reducing the terminal flow rate implies a decrease in late-stage energy input, necessitating a balance between displacement demand and energy input costs. This study aims to identify an optimal terminal flow rate that ensures efficient hydrocarbon displacement in the later stages while minimizing unnecessary energy input, thereby achieving the synergistic maximization of energy efficiency and total hydrocarbon production.

2.5 Dynamic oxygen content

Building on the three-parameter combination of gas injection rate (adjustment time, decay rate, and terminal flow rate), the dynamic regulation of oxygen content and flow rate in the early production stage can further enhance the development efficiency of autothermic pyrolysis *in-situ* conversion. To investigate the impact of time-responsive dual-parameter coupled regulation of oxygen content and injection rate on the reaction process, this study constructs a dual-parameter coupled regulation model, as illustrated in Fig. 5. In the reaction initiation stage, a high-oxygen low-flow strategy is adopted: The initial oxygen content is set to 100% with an injection rate of 100 m^3/day. The oxygen content linearly decreases to the air baseline value of 21%, and the injection rate is simultaneously increased gradually to 1,300 m^3/day. Different time points correspond to regulation nodes where the oxygen content returns to air levels and the flow rate reaches the optimal constant value. During this phase, the rapid dilution of oxygen content and sustained enhancement of flow rate establish a dual driving force mechanism, effectively promoting the thermal initiation efficiency of the reaction system. In the mid-stage reaction, the dynamic regulation framework of the injection rate is extended, implementing a secondary flow rate optimization: The flow rate decreases from 1,300 m^3/day to the terminal steady-state value at the optimal adjustment time and decay rate.

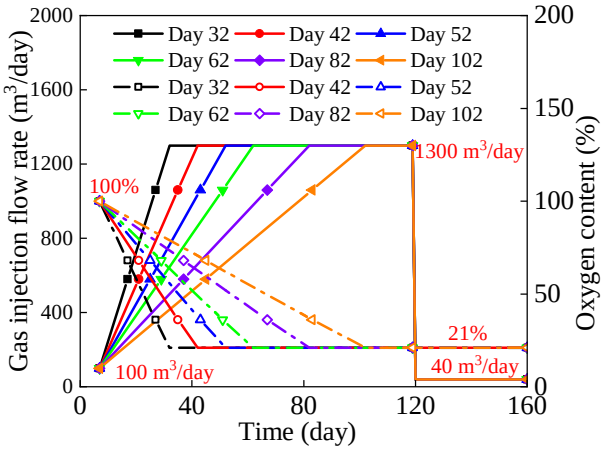

Fig. 5. Synergistic regulation function of dynamic oxygen content and gas injection flow rate.

3. Results and discussion

3.1 Optimization of constant gas injection rate

Different constant gas injection rates (1,000-1,500 m^3/day) exhibit distinct impacts on the development performance. As shown in Fig. 6, the cumulative gas production of all groups converges at approximately 16,000 m^3/m, indicating limited long-term variation in gas production due to the flow rate differences. However, the 1,300-1,500 m^3/day group demonstrates marginally superior gas production owing to a higher displacement intensity. The 1,300 m^3/day group achieves the highest energy efficiency peak of 5.97, making it the optimal choice, while the 1,000 m^3/day group attains a comparable energy efficiency peak of 5.96 and yields the highest oil production (29.18 m^3/m). Nevertheless, the 1,300 m^3/day group reaches its peak approximately 100 days earlier than the 1,000 m^3/day group, reflecting higher production efficiency.

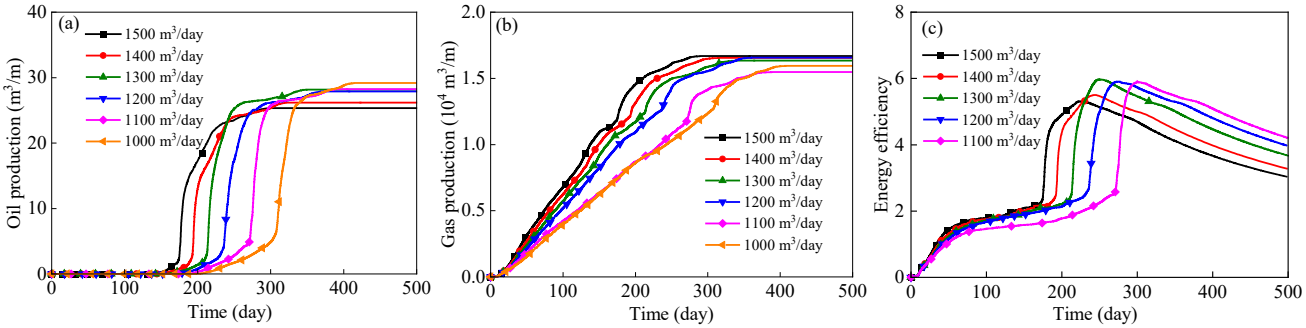

Fig. 6. Development performance under different constant gas injection flow rates: (a) Oil production, (b) gas production and (c) energy efficiency.

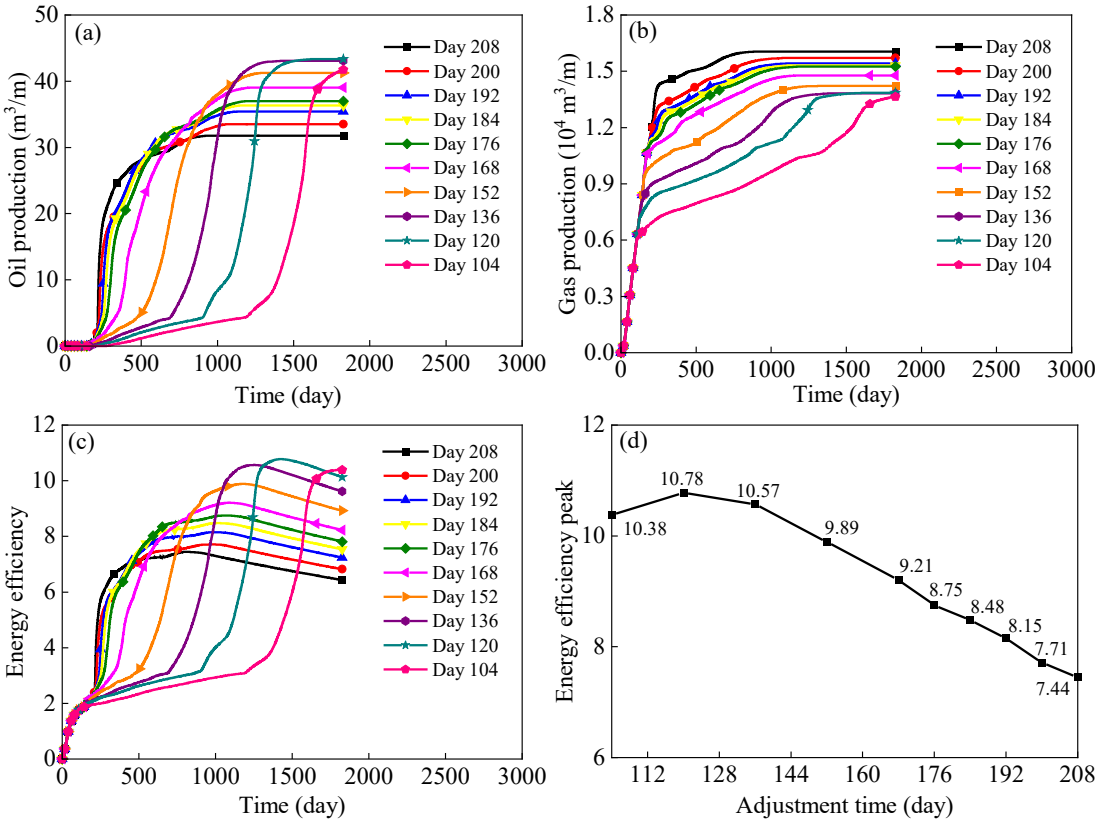

Fig. 7. Development performance under different adjustment times: (a) Oil production, (b) gas production, (c) energy efficiency and (d) energy efficiency peak.

Overall, the 1,300 m^3/day group combines sustained high oil production (28.16 m^3/m) with the highest energy efficiency and earlier peak response, thereby it is identified as the optimal constant gas injection rate scheme.

3.2 Dynamic regulation of gas injection rate

3.2.1 Optimization of adjustment time

Variations in the adjustment time (Day 104-208) significantly influence the development performance of kerogen pyrolysis. As illustrated in Fig. 7(b), shorter adjustment times correspond to lower cumulative gas production: The 208-day group yields 16,050 m^3/m, while the 104-day group produces only 13,640 m^3/m. An earlier flow rate reduction decreases the total injected gas volume, resulting in insufficient gas output. Fig. 7(a) shows that oil production initially increases then declines with shorter adjustment times, peaking at 43.3 m^3/m for the 120-day group, which represents a 53.76% increase compared to the optimal constant flow rate group (28.16 m^3/m). Figs. 7(c) and 7(d) demonstrate that the energy efficiency peak first rises then falls with reduced adjustment times, reaching a maximum of 10.78 for the 120-day group, which is 80.57% higher than the optimal constant flow rate group (5.97). These results indicate that the kerogen pyrolysis reaction stabilizes around day 120, where autothermic pyrolysis effects effectively sustain the process alongside substantial hydrocarbon production. Significantly reducing the gas injection

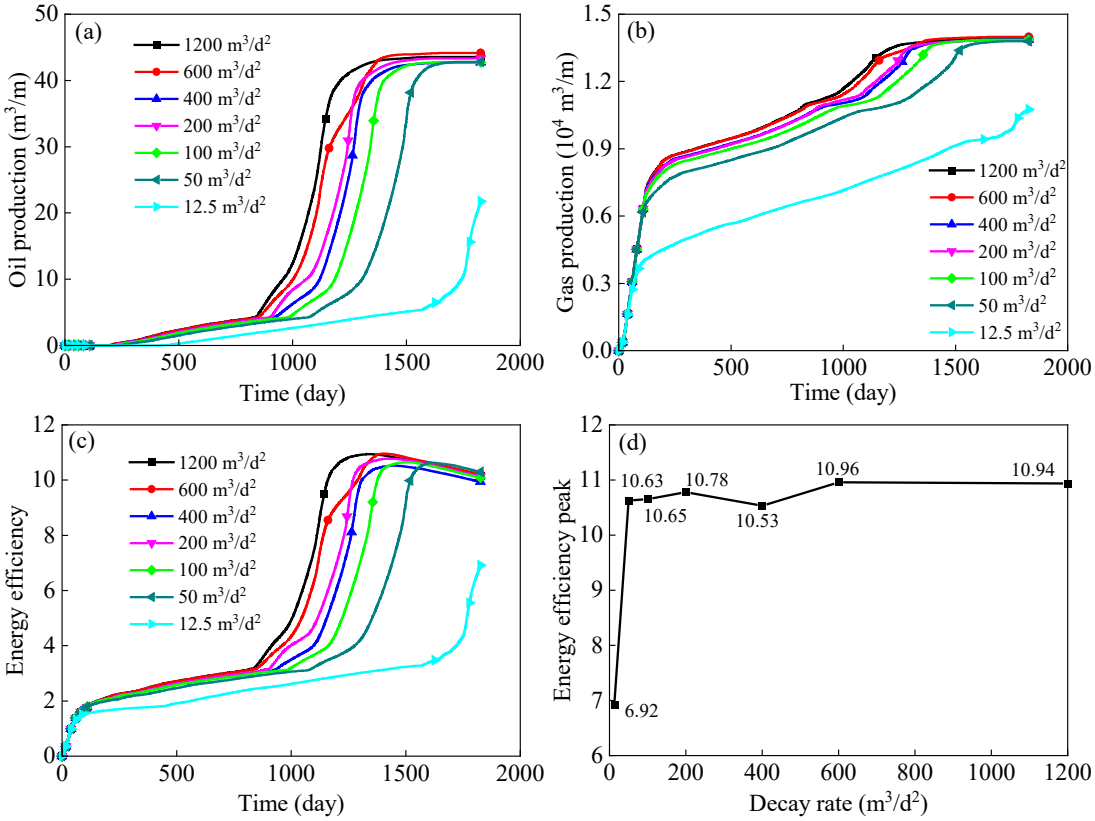

Fig. 8. Development performance under different decay rates: (a) Oil production, (b) gas production, (c) energy efficiency and (d) energy efficiency peak.

rate at this stage minimizes cumulative compression energy input and suppresses oxidative losses of hydrocarbons, thereby simultaneously enhancing energy efficiency and oil production. However, adjustment times shorter than day 120 (day 104) lead to declines in both energy efficiency peak (10.38) and oil production (41.7 m^3/m), as a premature flow rate reduction causes inadequate formation heating and restricts pyrolysis zone expansion. Due to its attainment of the highest energy efficiency, an adjustment time of day 120 is selected as the optimal value for this parameter. The determination of this optimal value also serves to define the critical time window for significant hydrocarbon production. Consequently, the subsequent optimization of the remaining two parameters (decay rate and terminal flow rate) was conducted based on this established temporal benchmark.

3.2.2 Optimization of decay rate

Based on the optimal adjustment time of day 120, the subsequent optimization of the decay rate further enhances production efficiency. As shown in Fig. 8(a), oil production reaches its highest levels at decay rates of 600 and 1,200 m^3/d^2 (44.1 and 43.5 m^3/m, respectively), with a difference of less than 2%, indicating extremely low sensitivity of oil production to parameter variations within the high decay rate range. Fig. 8(b) shows that gas production also peaks at 600 m^3/d^2 (13,980 m^3/m), while the 1,200 m^3/d^2 group yields 13,890 m^3/m, which represents a difference of less than 1%, further confirming the stability of hydrocarbon production in this interval. Figs. 8(c) and 8(d) demonstrate that the energy efficiency peak for the 1,200 m^3/d^2 and 600 m^3/d^2 groups are 10.94 and 10.96, respectively, differing by less than 0.5%. Notably, the 1,200 m^3/d^2 group achieves peak production 96 days earlier than the 600 m^3/d^2 group, highlighting its superior temporal efficiency under minimal compromise in hydrocarbon production or energy efficiency. In contrast, at a decay rate of 12.5 m^3/d^2, oil production drops to 21.7 m^3/m and the energy efficiency peak declines to 6.92. While high decay rates exhibit low sensitivity in energy efficiency peak variation, excessively low decay rates ($|k| < 50$ m^3/d^2) result in insufficient oxygen content in the formation during the initial reaction stage, leading to temperature decline, uneven thermal distribution, the suppression of kerogen cracking reactions, and the restricted evolution of porosity and permeability, which significantly reduces both energy efficiency and hydrocarbon production. Precisely because the adjustment time was fixed at day 120, an excessively low decay rate would lead to a premature reduction in the gas injection flow rate, thereby resulting in a significant decrease in oxygen concentration during the early production stage. Considering the dynamic responses of oil/gas production and energy efficiency, a decay rate of 1,200 m^3/d^2 is identified as the optimal solution within the current parameter system, ensuring high productivity and energy efficiency while maximizing temporal efficiency.

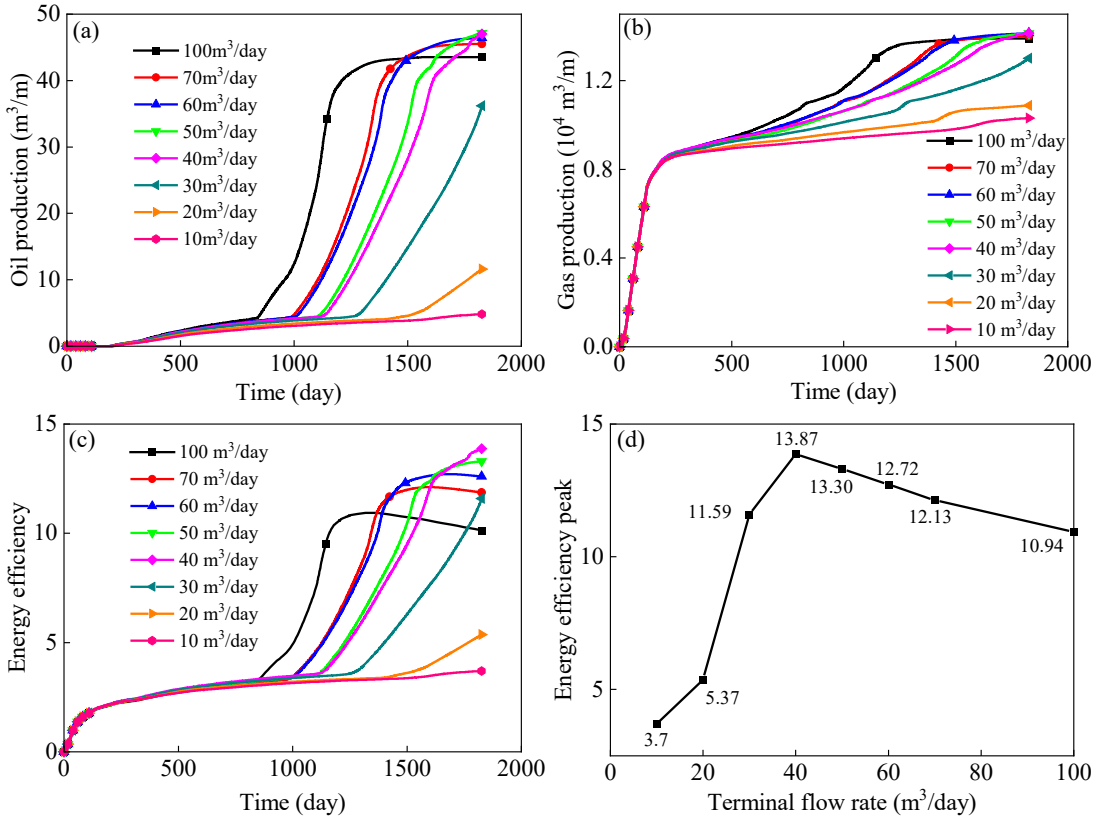

Fig. 9. Development performance under different terminal flow rates: (a) Oil production, (b) gas production, (c) energy efficiency and (d) energy efficiency peak.

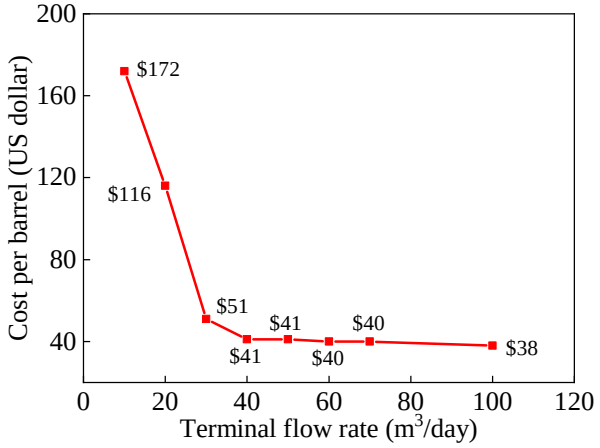

Fig. 10. Cost per barrel at the energy efficiency peak for different terminal flow rates.

3.2.3 Optimization of terminal flow rate

Building upon the optimal adjustment time of day 120 and the optimal decay rate of 1,200 m^3/d^2, the final optimization of the terminal flow rate will further reduce inefficient energy input and the oxidation loss of hydrocarbon products. As shown in Fig. 9(a), as the terminal flow rate declines from 10 to 100 m^3/day, oil production initially increases then decreases. The 50 m^3/day group achieves the maximum oil production of 47.1 m^3/m, while the 40 m^3/day group yields 47.0 m^3/m, which represents a difference of less than 1%. This indicates the low sensitivity of oil production to terminal flow rate within the 40-50 m^3/day range, with both values approaching the optimal level. Fig. 9(b) demonstrates that gas production first slightly increases then declines rapidly with reduced terminal flow rates, peaking at 14,150 m^3 for the 40 m^3/day group, significantly exceeding other groups. Figs. 9(c) and 9(d) show that the energy efficiency peak initially rises then falls as the terminal flow rate decreases from 10 to 100 m^3/day, reaching a maximum of 13.87 for the 40 m^3/day group, which represents a 132.33% enhancement compared to the optimal constant flow rate group (5.97). Concurrently, oil production increases by 66.9% relative to the constant flow rate group (28.16 m^3/m). These results highlight the dual advantages of dynamic regulation in energy utilization efficiency and hydrocarbon recovery. After the autothermic pyrolysis reaction stabilizes, a lower terminal flow rate prevents excessive organic consumption caused by overexpansion of the kerogen pyrolysis zone, ensuring long-term production stability. Simultaneously, this parameter significantly reduces cumulative compression energy during the mid-to-late production stages, maximizing energy efficiency.

A comprehensive analysis of the development performance across terminal flow rate groups reveals that while the 30, 20 and 10 m^3/day groups may achieve gradual improvements in energy efficiency over extended periods due to sustained autothermic pyrolysis reactions, their peak hydrocarbon production and energy efficiency within practical engineering

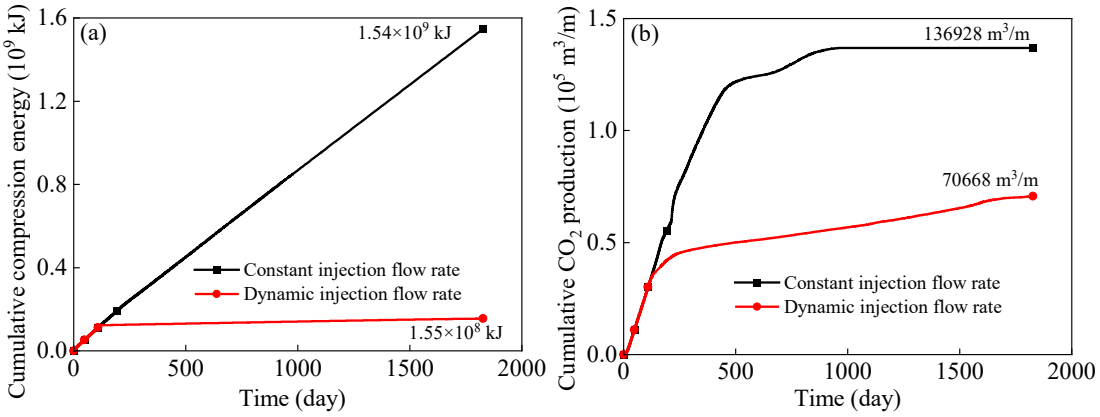

Fig. 11. Cumulative compression energy and CO_2 production under constant and optimal gas injection parameters: (a) Cumulative compression energy and (b) cumulative CO_2 production.

cycles remain significantly lower than those of the 40 m^3/day group. To quantitatively evaluate the economic disparities, the cost per barrel is introduced as a key metric, integrating economic inputs such as labor and electricity expenditures during development to reflect the economic cost per unit of oil produced. As shown in Fig. 10, the cost per barrel at the energy efficiency peak exhibits a distinct nonlinear trend across terminal flow rates: When the flow rate drops below 40 m^3/day, costs surge sharply, reaching 172, 116 and 51 USD/barrel for the 10, 20 and 30 m^3/day groups, respectively, far exceeding the 41 USD/barrel of the 40 m^3/day group. In contrast, for flow rates above 40 m^3/day, the costs stabilize near 40 USD/barrel across the 50-100 m^3/day groups. This cost divergence stems from the compatibility of flow rate with thermal reaction efficiency. The 40 m^3/day group achieves optimal alignment between gas injection volume and reservoir thermal reaction rates, ensuring high energy conversion efficiency while avoiding accumulated inefficiencies from excessively low flow rates. Thus, considering both project duration constraints and economic indicators, the 40 m^3/day group emerges as the optimal solution, balancing short-term benefits with long-term potential through the lowest cost per barrel (41 USD/barrel) and balanced development efficiency.

The dynamic regulation of gas injection rate during the mid-to-late production stages results in a significant reduction in both energy input and oxidation losses of hydrocarbons. The cumulative compression energy and CO_2 production under constant flow rate and optimal gas injection flow rate parameters are presented in Fig. 11. The dynamic regulation of gas injection flow rates significantly reduces the cumulative compression energy from 1.54×10^9 kJ in the constant flow rate group to 1.55×10^8 kJ, achieving a 90% reduction, which demonstrates effective energy input minimization and enhanced energy utilization efficiency. Meanwhile, cumulative CO_2 production decreases from 136,928 m^3/m in the constant flow rate group to 70,668 m^3/m, constituting a 48% decline, which further confirms the significant reduction in hydrocarbon oxidation losses during the autothermic pyrolysis process.

3.3 Dynamic oxygen content regulation

3.3.1 Impact of oxygen-flow synergistic regulation

The synergistic regulation of oxygen content and gas injection rate during the initial reaction stage further reduces energy input and advances the onset of pyrolysis. Fig. 12 illustrates the development performance under the synergistic regulation of oxygen content and flow rate. The 52-day time point is identified as the optimal control node for restoring oxygen content to the atmospheric level (21%) and the flow rate to the optimal constant value (1,300 m^3/day). At this stage, oil production peaks at 41.55 m^3/m, while the energy efficiency simultaneously reaches its maximum value of 14.80. Gas production (14,116 m^3/m) differs by only 1.84% from the 62-day value (14,376 m^3/m), indicating a dynamic equilibrium among energy conversion efficiency and output on day 52. Through synergistic oxygen-flow regulation, the energy efficiency peak (14.80) increases by 6.71% compared to the optimal gas injection flow rate parameters (peak: 13.87). This value significantly exceeds the conventional oil shale development level (generally below 3%), demonstrating technical feasibility for industrial-scale production. The high initial oxygen concentration promotes rapid kerogen cracking, accelerating the evolution of the temperature field and permeability, thus advancing the oil production period and shortening the cycle. As the oxygen content decreases to atmospheric level, maintaining an optimal dynamic control of gas injection flow rate further enhances both energy efficiency and oil production.

Restoration to atmospheric oxygen content and 1,300 m^3/day flow rate prior to day 52 may lead to insufficient kerogen cracking rates due to premature oxygen reduction, failing to fully establish high-temperature fields and permeability and thereby limiting rapid oil release. Although an initial high oxygen content (100%) combined with low flow rate (100 m^3/day) accelerates reaction initiation, premature return to atmospheric level (21%) may compromise mid-term energy supply continuity, preventing energy efficiency from reaching higher levels. Conversely, delayed restoration beyond day 52 risks prolonged low flow rate, keeping the reaction in a transitional phase. This delays autothermic pyrolysis reaction rates during the mid-term, failing to sustain high reservoir temperatures and impairing hydrocarbon output. On

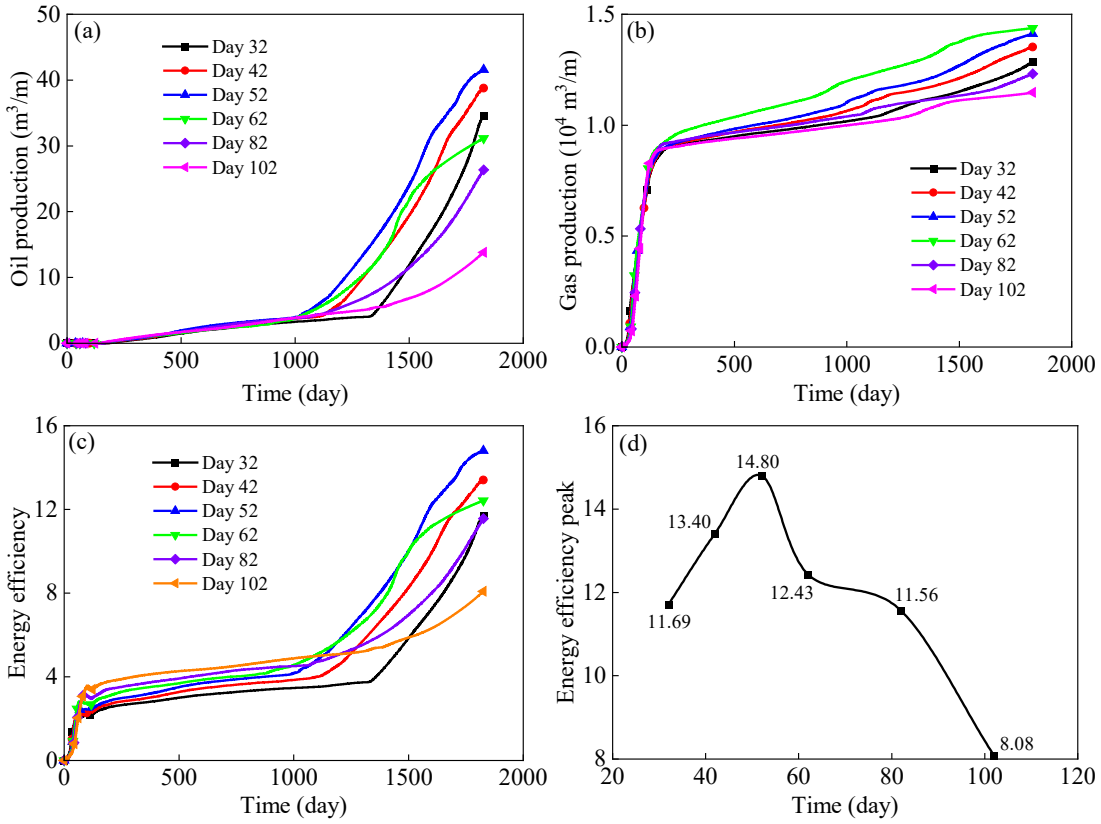

Fig. 12. Development performance under oxygen-flow synergistic regulation: (a) Oil production, (b) gas production, (c) energy efficiency and (d) energy efficiency peak.

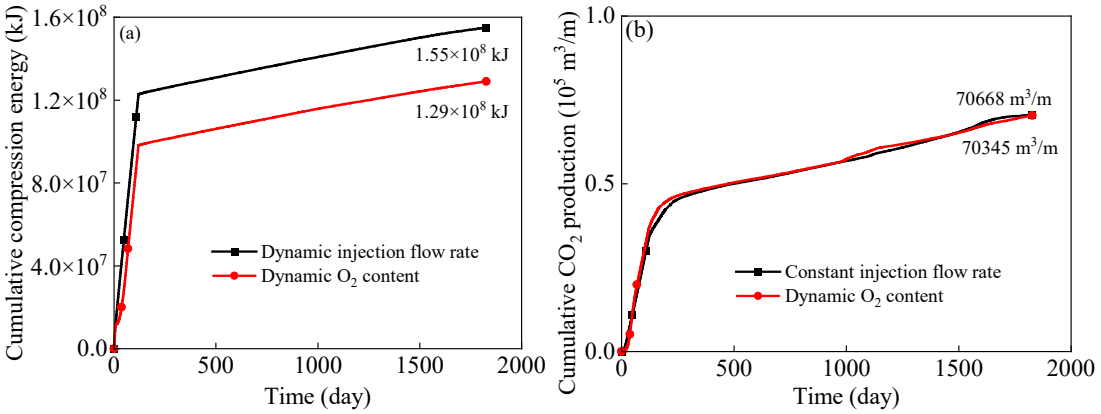

Fig. 13. Cumulative compression energy and CO_2 production under oxygen-flow synergistic regulation: (a) Cumulative compression energy and (b) cumulative CO_2 production.

day 62, the energy efficiency peak (12.43) and oil production (31.17 m^3/m) were markedly lower than day 52, confirming that delayed restoration reduces the system energy conversion efficiency and production potential.

The utilization of high-oxygen, low-flow rate gas injection during the initial reaction stage leads to a further reduction in compression energy loss. As shown in Fig. 13, the final cumulative compression energy for the dynamic gas injection flow rate regulation scheme is 1.55×10^8 kJ, while the oxygen-flow synergistic regulation scheme reduces it to 1.29×10^8 kJ, representing an additional 16% decrease in energy input and highlighting the critical role of the initial reaction phase in overall energy efficiency. Meanwhile, cumulative CO_2 production under oxygen-flow synergistic regulation decreases slightly from 70,345 to 70,668 m^3/m. During the pre-stable initial phase of autothermic pyrolysis reactions, the combination of high oxygen content and low flow rate accelerates reaction preheating via enhanced oxidation rates, promoting earlier autothermic pyrolysis initiation. Simultaneously, the low flow rate effectively suppresses the excessive oxidation of organic matter. Consequently, although CO_2 production shows minimal change, this strategy significantly reduces energy in-

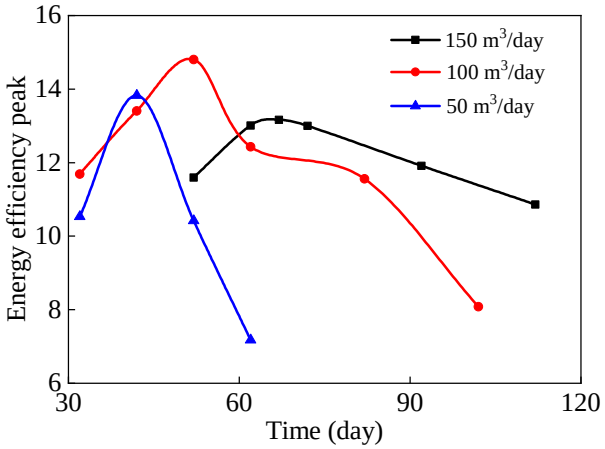

Fig. 14. Effect of different initial flow rates on the energy efficiency peak.

put while maintaining low oxidation losses, thereby further increasing the energy efficiency.

3.3.2 Impact of initial flow rate

The initial flow rate of the high-oxygen, low-flow-rate gas injected during the initial reaction stage affects both the magnitude and the time to peak energy efficiency. The influence of different initial gas injection flow rates on the energy efficiency peak is presented in Fig. 14. When the initial flow rate is set to 50, 100 and 150 m^3/day, the energy efficiency peak occurs day 42, 52 and 67, respectively, with peak values of 13.16, 14.80 and 13.83. This indicates that lower initial flow rates correspond to earlier optimal control nodes, while the 100 m^3/day condition yields the highest energy efficiency peak. The temporal offset of the optimal control node primarily stems from the regulation of thermal field expansion rate by the flow rate. Lower flow rates (50 m^3/day) establish stable thermal gradients through slow heating, enabling continuous kerogen pyrolysis within the ideal thermal cracking range (typically 300-400°C), thereby achieving higher energy accumulation efficiency and earlier peak occurrence. Moderate flow rates (100 m^3/day) precisely match the oxygen diffusion rate with pyrolysis demand during the initial reaction phase, accelerating kerogen cracking via high oxygen concentration to shorten the oil production period while maintaining thermal energy utilization efficiency through subsequent dynamic regulation. In contrast, excessively high flow rates (150 m^3/day) induce localized overheating, triggering secondary cracking, and result in an oxygen surplus that promotes oxidative side reactions. These factors not only increase compression energy input but also reduce thermal energy utilization efficiency, leading to the latest peak occurrence.

The highest energy efficiency peak under 100 m^3/day conditions is attributed to the optimal coupling of the thermal-oxygen-reaction system. This flow rate ensures sufficient initial oxygen diffusion to meet rapid kerogen pyrolysis demands and avoids late-stage energy waste through dynamic regulation, achieving the best balance between thermal energy conversion efficiency and oil production. In contrast, while 50 m^3/day results in an earlier peak, its limited pyrolysis scale restricts overall energy output; the initial advantages of 150 m^3/day are offset by excessive energy losses, resulting in a lower energy efficiency peak compared to the moderate flow rate condition.

Under different initial flow rates, the diffusion range of the temperature field during the initial reaction stage varies, which in turn affects the kerogen pyrolysis reaction and the porosity evolution of the formation. As shown in Fig. 15, the thermal field evolution under an initial flow rate of 100 m^3/day exhibits optimal performance: The thermal front propagates farther and distributes more uniformly, significantly outperforming the other two cases. The 50 m^3/day case shows restricted diffusion rates, while the 150 m^3/day case suffers from heterogeneity damage due to localized overheating. Fig. 16 illustrates the kerogen concentration evolution. The 100 m^3/day case achieves the farthest and most uniform pyrolysis zone expansion; in contrast, the 150 m^3/day case exhibits a deeper central depression despite a larger pyrolysis area, reflecting the risk of organic matter over-combustion triggered by intense autothermic pyrolysis under high initial oxygen levels. The 50 m^3/day case shows limited pyrolysis zone extension due to insufficient preheating. Fig. 17 reveals structural degradation under high flow rates. While the 150 m^3/day case attains the largest porosity expansion range, localized clogging zones emerge on the right side of the pyrolysis region. Conversely, the 100 m^3/day and 50 m^3/day cases maintain more uniform pore structure evolution. The clogging mechanism stems from an imbalance between excessive initial flow rate and oxygen supply, inducing violent pyrolysis reactions accompanied by volatile release and coke formation, which disrupts pore homogeneity. Furthermore, high oxygen levels exacerbate oxidative side reactions, generating localized high temperatures (evidenced by abrupt near-field temperature spikes in the 150 m^3/day group) that cause pore collapse or coke accumulation, hindering hydrocarbon migration and increasing loss risks. In comparison, the 100 m^3/day case optimizes the match between oxygen diffusion and pyrolysis demand, avoiding over-combustion while preserving pore uniformity, thereby achieving superior performance in energy efficiency, pyrolysis efficiency and pore connectivity.

3.4 Comparison of key technologies

The dynamic control strategy for injection and production parameters proposed in this study inherits the core advantages of existing research while effectively overcoming its technical bottlenecks, demonstrating significant improvements in comprehensive performance and technical reliability. Previous studies have laid a crucial foundation by revealing the synergistic effect between oxygen concentration and injection rate, constructing efficient heat transfer and utilization mechanisms and enhancing energy efficiency through auxiliary fuels. This strategy avoids the risks associated with fixed or inappropriate parameters, such as inefficient energy input, oxidative consumption of products, reaction termination, and gas channeling, thereby significantly improving energy utilization efficiency, achieving superior techno-economic viability, and shortening the investment payback period. A detailed comparison of these technologies is presented in Table 5.

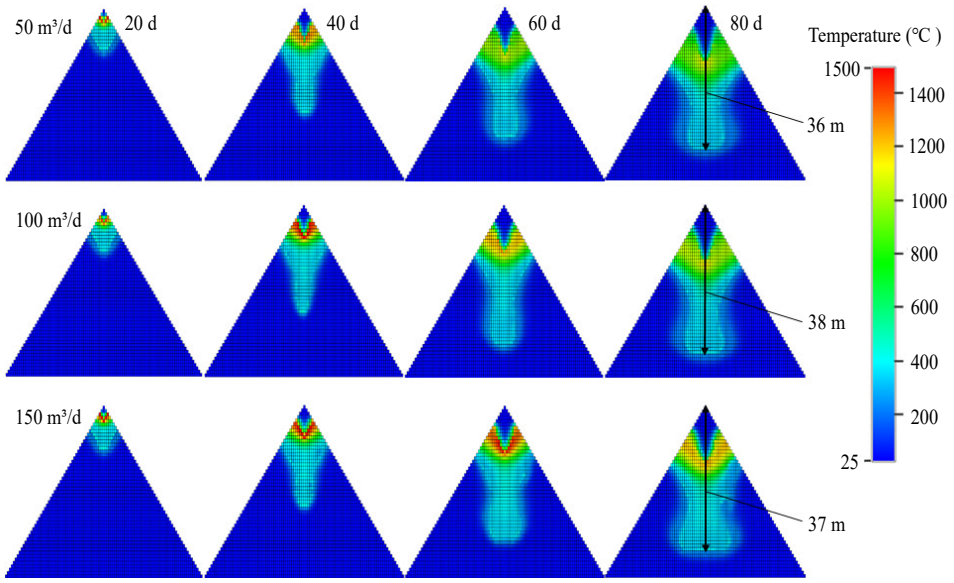

Fig. 15. Temperature field evolution under different initial flow rates.

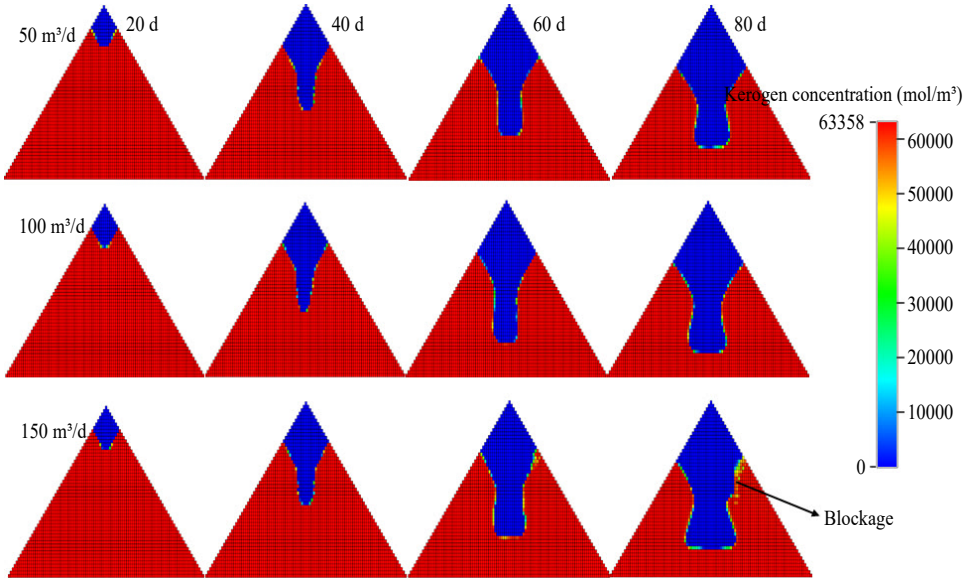

Fig. 16. Kerogen concentration evolution under different initial flow rates.

4. Conclusions

This study develops a dynamic optimization model for the injection-production parameters of the autothermic pyrolysis *in-situ* conversion process of oil shale, and determines the optimal combination of gas injection parameters. Under this parameter system, a synergistic regulation of oxygen content and flow rate during the pyrolysis initiation phase further enhances reaction initiation efficiency and hydrocarbon displacement capacity, ultimately establishing a dynamic regulation framework that synergistically improves both energy efficiency and hydrocarbon output. The primary conclusions are as follows:

1) The optimal flow parameter combination is established as an adjustment time of day 120, a decay rate of 1,200 m^3/d^2, and a terminal flow rate of 40 m^3/day. Compared to traditional constant gas injection, this combination reduces cumulative compression energy by 90% and CO_2 production by 48%, while it increases oil production by 66.9% to 47 m^3/m. The energy efficiency peak reaches 13.87, representing a 132.33% improvement over the constant flow rate group, effectively suppressing gas channeling and hydrocarbon oxidation losses.
2) Building upon the optimized gas injection flow rate, the synergistic regulation of oxygen content and flow rate during the initiation phase further elevates the energy efficiency peak to 14.80 while maintaining high hydrocarbon production efficiency. This represents an additional 6.71% increase compared to the flow-rate-only optimization group, with a further 16% reduction in cumulative com-

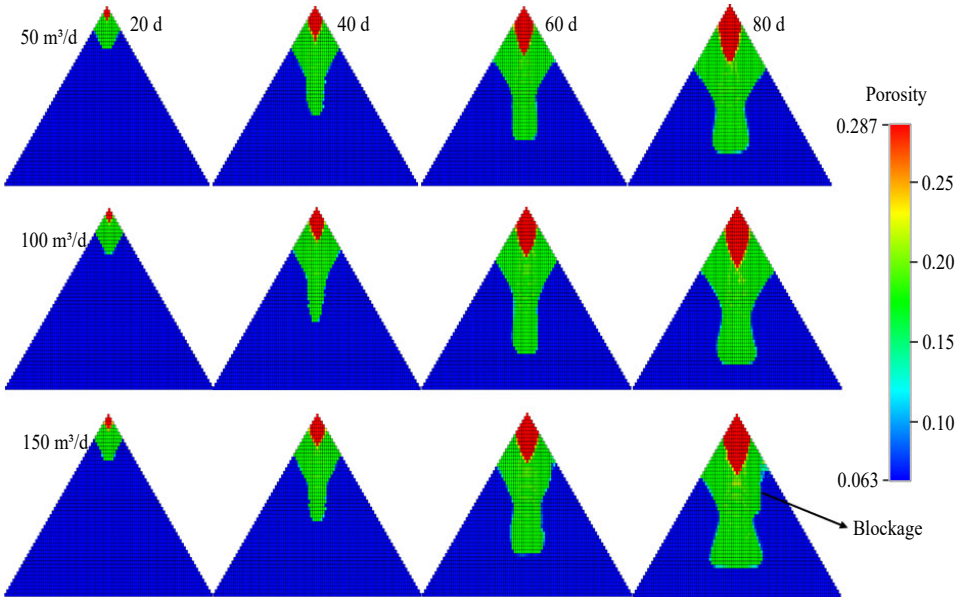

Fig. 17. Porosity evolution under different initial flow rates.

Table 5. Comparison of existing technologies.

Control strategy	Key parameters	Key advantages	Major drawbacks
Impact of gas injection parameters on the autothermal pyrolysis in-situ conversion process (Yang et al., 2023b)	Oxygen concentration and gas injection rate	Elucidates the synergistic effect between oxygen concentration and gas injection rate	High oxidative loss
Autothermal pyrolysis in-situ conversion process (Guo et al., 2023a)	Preheating temperature, oxygen concentration and gas injection rate	Efficient heat transfer and utilization	Stringent requirements for parameter matching
Natural gas-assisted autothermal pyrolysis (Zhu et al., 2026)	Mixing ratio of natural gas in the injection gas	Significantly enhances energy efficiency	Moderate adaptability in high oil-bearing formations
Dynamic control of injection-production parameters	Oxygen concentration and gas injection rate	Relatively high energy efficiency, favorable techno-economic viability and time efficiency	Relatively high precision requirements for parameter control

pression energy, highlighting the critical role of initial-phase regulation on overall energy efficiency.

3) By matching the characteristics of the pyrolysis reaction stages, the dynamic regulation strategy effectively inhibits gas channeling and hydrocarbon oxidation losses and optimizes the propagation of the reservoir thermal field and the evolution of pore structure. Post-optimization, the energy efficiency is enhanced to above 10, the cost per barrel is reduced to 41 USD/barrel, and the production cycle can be shortened by 96 days. These data demonstrate favorable technical economics and time efficiency, indicating the significant potential of the proposed strategy for industrial application.

Acknowledgements

We acknowledge the financial support offered by the National Oil Shale Exploitation R&D Center Open Fund Project (No. 33550000-24-ZC0613-0055) and the Science and Technology Research Project of the Education Department of Jilin Province (No. JJKH20261702KJ).

Conflicts of interest

The authors declare no competing interest.

References

Alshareef, A. H., Scherer, A., Tan, X., et al. Formation of archipelago structures during thermal cracking implicates a chemical mechanism for the formation of petroleum asphaltenes. Energy & Fuels, 2011, 25: 2130.

Brandt, A. R. Converting oil shale to liquid fuels: Energy

inputs and greenhouse gas emissions of the Shell in situ conversion process. Environmental Science & Technology, 2008, 42(19): 7489-7495.

Braun, R. L., Burnham, A. K. PMOD: a flexible model of oil and gas generation, cracking, and expulsion. Organic Geochemistry, 1992, 19(1): 161-172.

Dong, F., Feng, Z., Yang, D., et al. Permeability evolution of pyrolytically-fractured oil shale under in situ conditions. Energies, 2018, 11(11): 3033.

Du, M., Yang, Z., Feng, C., et al. Microscopic production characteristics of pore crude oil and influencing factors during enhanced oil recovery by air injection in shale oil reservoirs. ACS Omega, 2023, 8(20): 18186-18201.

Fan, D. Research on paleoclimate, paleoenvironment and source rock development model of the cretaceous Shahezi Formation in Xujiaweizi fault depression, Songliao Basin. Changchun, Jilin University, 2022. (in Chinese)

Gao, Y., Wan, T., Dong, Y., et al. Numerical and experimental investigation of production performance of *in-situ* conversion of shale oil by air injection. Energy Reports, 2022, 8: 1099-1112.

Guo, W., Li, Q., Deng, S., et al. Mechanism and reservoir simulation study of the autothermic pyrolysis *in-situ* conversion process for oil shale recovery. Petroleum Science, 2023a, 20(2): 1053-1067.

Guo, W., Sun, Y., Li, Q., et al. Oil shale *in-situ* conversion technology triggered by topochemical reaction method and pilot test project in Songliao Basin. Acta Petrolei Sinica, 2024, 45(7): 1104-1121+1129. (in Chinese)

Guo, W., Yang, Q., Deng, S., et al. Experimental study of the autothermic pyrolysis *in-situ* conversion process (ATS) for oil shale recovery. Energy, 2022, 258: 124878.

Guo, W., Zhang, X., Sun, Y., et al. Migration mechanism of pyrolysis oil during oil shale in situ pyrolysis exploitation. Energy, 2023b, 285: 128769.

He, H., Liu, Y., Zhao, G., et al. Investigation of in situ gelation behavior and enhanced oil recovery ability of polymer gel used for controlling CO_2 channeling in tight fractured reservoir. Gels, 2024, 10(11): 741.

He, W., Sun, Y., Guo, W., et al. Organic geochemical characteristics of the upper cretaceous Qingshankou Formation oil shales in the Fuyu Oilfield, Songliao Basin, China: Implications for oil-generation potential and depositional environment. Energies, 2019, 12(24): 4778.

He, W., Sun, Y., Shan, X. Organic matter evolution in pyrolysis experiments of oil shale under high pressure: Guidance for in situ conversion of oil shale in the Songliao Basin. Journal of Analytical and Applied Pyrolysis, 2021, 155: 105091.

Jia, B., Huang, Z. Oil shale in situ production using a novel flow-heat coupling approach. ACS Omega, 2024, 9(7): 7705-7718.

Jin, J., Deng, Y., Song, L., et al. Nanozeolite encapsulated single-atom catalysts: Synergetic *in-situ* conversion of oil shale using supercritical CO_2. SPE Journal, 2025, 30(8): 4814-4824.

Jin, J., Song, C., Sun, J., et al. ZnCl2-catalyzed low-temperature pyrolysis enabling efficient upgrading of Wangqing oil shale. Fuel, 2026, 420: 138926.

Khakimova, L., Bondarenko, T., Cheremisin, A., et al. High pressure air injection kinetic model for Bazhenov Shale Formation based on a set of oxidation studies. Journal of Petroleum Science and Engineering, 2019, 172: 1120-1132.

Lee, K. J., Finsterle, S., Moridis, G. J. Analyzing the impact of reaction models on the production of hydrocarbons from thermally upgraded oil shales. Journal of Petroleum Science and Engineering, 2018, 168: 448-464.

Li, J., Lang, Y., Li, B., et al. N2 influences on CH4 accumulation and displacement in shale by molecular dynamics. Scientific Reports, 2025a, 15(1): 1833.

Li, Q., Wang, X., Li, D., et al. Development and performance evaluation of multi-functional slickwater fracturing fluid system for shale reservoirs. Scientific Reports, 2025b, 15(1): 17637.

Liu, Y., Xue, L., Bai, F., et al. Three-dimensional numerical simulation of hydrocarbon production and reservoir deformation of oil shale in situ conversion processing using a downhole burner. ACS Omega, 2022, 7(27): 23695-23707.

Lu, Y., Wang, Z., Kang, Z., et al. Comparative study on the pyrolysis behavior and pyrolysate characteristics of Fushun oil shale during anhydrous pyrolysis and sub/supercritical water pyrolysis. RSC Advances, 2022, 12(26): 16329-16341.

Ma, C., Tan, F., Qin, J., et al. Study on the difference in CO_2 and air injection in the fracture/matrix dual medium of continental shale reservoirs. ACS Omega, 2023, 8(22): 20020-20030.

Pei, S., Wang, Y., Zhang, L., et al. An innovative nitrogen injection assisted *in-situ* conversion process for oil shale recovery: Mechanism and reservoir simulation study. Journal of Petroleum Science and Engineering, 2018, 171: 507-515.

Shakib, J. T., Akhgarian, E., Ghaderi, A. The effect of hydraulic fracture characteristics on production rate in thermal EOR methods. Fuel, 2015, 141: 226-235.

Sun, W., Liu, X., Zhan, T., et al. Quality characteristics of oil shale of the 1st member of upper cretaceous Qingshankou Formation of well JFD3 in southeastern rising area of Songliao Basin. Jilin Geology, 2022, 41(2): 18-23. (in Chinese)

Tian, H., Guo, W., Li, Q., et al. High-pressure pyrolysis mechanism of tar-rich coal in Taiyuan Formation, Ordos Basin. Energy, 2025, 337: 138675.

Tong, J., Han, X., Wang, S., et al. Evaluation of structural characteristics of Huadian oil shale kerogen using direct techniques (Solid-State 13C NMR, XPS, FT-IR, and XRD). Energy & Fuels, 2011, 25(9): 4006-4013.

Wang, E., Guo, T., Li, M. Paleosedimentary environmental reconstruction and mechanisms of the response to the Toarcian OAE in a lacustrine shale system. Scientific Reports, 2024a, 14(1): 14082.

Wang, G., Yang, D., Zhao, Y., et al. Experimental investigation on anisotropic permeability and its relationship with anisotropic thermal cracking of oil shale under

high temperature and triaxial stress. Applied Thermal Engineering, 2019, 146: 718-725.

Wang, L., Gao, C., Xiong, R., et al. Development review and the prospect of oil shale *in-situ* catalysis conversion technology. Petroleum Science, 2024b, 21(2): 1385-1395.

Wang, L., Yang, D., Zhao, Y., et al. Evolution of pore characteristics in oil shale during pyrolysis under convection and conduction heating modes. Oil Shale, 2020, 37(3): 224-241.

Wang, W. Establishment and application of evaluation criteria of shale oil and gas resources potential: A case of southern Songliao Basin. Daqing, Northeast Petroleum University, 2013. (in Chinese)

Wang, Y., Ren, S., Zhang, L., et al. Numerical study of air assisted cyclic steam stimulation process for heavy oil reservoirs: Recovery performance and energy efficiency analysis. Fuel, 2018, 211: 471-483.

Wang, Y., Kang, S., Jiao, L., et al. Catalytic hydrothermal pyrolysis behaviors of oil shale under restrained conditions. Scientific Reports, 2025, 15(1): 21276.

Wu, A., Wu, J., Chen, L., et al. Recent progress on in situ catalytic conversion catalysts for oil shale. ACS Omega, 2024, 9(35): 36904-36916.

Xie, X., Hu, L., Deng, H., et al. Evolution of pore structure and fractal characteristics of marine shale during electromagnetic radiation. Plos One, 2020, 15(10): e0239662.

Xu, S., Lü, X., Sun, Y., et al. Optimization of temperature parameters for the autothermic pyrolysis *in-situ* conversion process of oil shale. Energy, 2023, 264: 126309.

Yang, F., Cheng, X., Li, M., et al. Numerical investigation of the heat and mass transfer during the in situ pyrolysis process of oil-rich coal. Processes, 2023a, 11(11): 3226.

Yang, Q., Guo, W., Xu, S., et al. The autothermic pyrolysis *in-situ* conversion process for oil shale recovery: Effect of gas injection parameters. Energy, 2023b, 283: 129134.

Yan, Z., Ji, H., Guo, G., et al. Geochemical characteristics of trace elements and REEs and their geological significance for uranium mineralization within the Qianjiadian sandstone-hosted uranium deposit, Songliao Basin. Geofluids, 2023, 2023: 6297033.

Zhang, L., Chen, L., Hu, R., et al. Subsurface multiphase reactive flow in geologic CO_2 storage: Key impact factors and characterization approaches. Advances in Geo-Energy Research, 2022, 6(3): 179-180.

Zhao, F., Yang, Z., Zhang, L., et al. The effect of temperature on pyrolysis products during oil shale thermal decomposition. Scientific Reports, 2025, 15(1): 26135.

Zhao, R., Xu, H., Sun, Z., et al. Study on the lower limits of physical parameters for heavy oil reservoirs during the in situ combustion process. ACS Omega, 2023, 8(6): 5995-6008.

Zhou, X., Li, H., Zeng, F., et al. Lightening of shale oil using high-temperature supercritical CO_2: An experimental study. Advances in Geo-Energy Research, 2025, 16(2): 99-113.

Zhu, C., Guo, W., Sun, Y., et al. Reaction mechanism and reservoir simulation study of the high-temperature nitrogen injection *in-situ* oil shale process: A case study in Songliao Basin, China. Fuel, 2022, 316: 123164.

Zhu, C., Jiang, T., Yao, S., et al. Numerical investigation of natural gas-enhanced autothermic pyrolysis for optimizing *in-situ* conversion in oil shale. Petroleum Science, 2026, 23(2): 762-776.